ELSEVIER

Journal of Nuclear Materials 241–243 (1997) 1082–1086

journal of nuclear materials

Hydrogen trapping in and release from tungsten: Modeling and comparison with graphite with regard to its use as fusion reactor material

P. Franzen *, C. Garcia-Rosales, H. Plank, V.Kh. Alimov [1]

Max-Planck-Institut für Plasmaphysik, EURATOM Association, P.O. Box 1533, D-85740 Garching, Germany

Abstract

Trapping and release of deuterium implanted in tungsten is investigated by modeling the results of reemission, thermal and isothermal desorption experiments. Rate coefficients and activation energies for diffusion, trapping and detrapping are derived. Hydrogen atoms are able to diffuse deep into tungsten, establishing a solute amount of the same order of magnitude as the trapped one. This 'diffusion zone' exceeds the implantation zone by more than two orders of magnitude, even at room temperature. The solute amount of hydrogen in tungsten depends only slightly on the incident ion energy, but scales with implantation fluence. This high amount of solute hydrogen is the main difference of tungsten compared to graphite where nearly all hydrogen is trapped in the implantation zone, the solute amount being orders of magnitude lower. The resulting unlimited accumulation of hydrogen in tungsten deep in the material down to the backward surface disadvantages tungsten as fusion reactor material with regard to hydrogen recycling properties.

Keywords: Wall pumping; High Z wall material; Wall particle retention; Wall impurity trapping; Tritium inventory and economy

1. Introduction

Apart from graphite and beryllium, the high Z material tungsten is considered as plasma facing material for ITER [1]. In order to provide an experimental data base for the ITER divertor, tungsten coated graphite tiles have been installed as divertor target plates in the tokamak ASDEX Upgrade for the experimental period December 1995 to July 1996 [2].

The hydrogen retention and recycling properties of a first wall material during and after the bombardment with hydrogen from the plasma are important factors controlling the particle balance and the isotopic composition of the plasma, as well as the tritium inventory of the vessel walls. The experimental data base [3–8] for hydrogen retention and release in and from tungsten during ion implantation and for rate coefficients like diffusion [9,10] is rather limited and partly contradictionary.

In this paper we study the recycling properties of deuterium implanted in tungsten with a wide range of energies (100 eV, 1.5 keV, 8 keV) and sample temperatures (300 K to 900 K) by modeling the results of reemission and thermal desorption (TDS) and isothermal desorption experiments. We derive rate coefficients for diffusion, recombination and trapping. The results are discussed in comparison to graphite with regard to the use as wall material in fusion devices.

2. Model

The model of hydrogen reemission and thermal release from tungsten is based on the model of hydrogen release from metals by Möller et al. [11]. The detailed mathematical description will be published elsewhere [12]. Shortly, the model assumes the hydrogen inventory of a metal to consist of a solute and trapped concentrations. Hydrogen

* Corresponding author. Tel.: +49-89 3299 1399; fax: +49-89 3299 2580; e-mail: pef@ipp-garching.mpg.de.

[1] Guest from the Institute of Physical Chemistry of the Russian Academy of Sciences, Moscow.

PII S0022-3115(96)00664-2

ions entering the metal are slowed down until they thermalize and may either be trapped at natural or ion induced traps, or may diffuse back to the surface or into the bulk. The release of hydrogen from a metal occurs as molecules after surface recombination. The atomic release of deuterium from tungsten above 1100 K [5] is not included in the model due to lower maximum temperatures achieved at the experiments [5].

In order to keep the number of fitting parameters as low as possible, further assumptions were made prior to the calculations:

– Only two traps are assumed: a natural trap, the concentration depending on the tungsten material but constant throughout the whole sample, and, in the case of implantation with sufficient ion energy, an ion induced trap, the concentration independent on material and ion energy, but restricted to the implantation zone. Trapping is limited by diffusion.

– For the case of keV implantation, where trapping sites can be generated by the ion beam, the sample was assumed to be preimplanted with the maximum trap concentration already established.

– All beam induced effects on the rate coefficients are neglected; especially, the diffusion coefficient in the implantation zone has the same value as beyond.

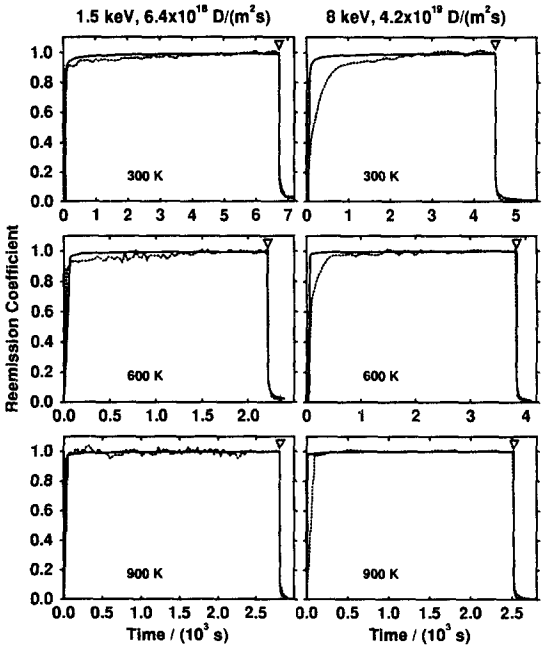

Fig. 1. Modeling of reemission data [3,4] for 1.5 keV and 8 keV D^+ implantation, respectively, of single crystal tungsten at 300 K, 600 K, and 900 K. Dotted lines denote experimental data, solid lines the computational results. Note the different time scales. The triangle denotes the ion beam termination time.

3. Computational results and discussion

Figs. 1–3 show the comparison of the model calculations, obtained with the parameter in Table 1, with some experimental results [3,4,6,13]. The experimental conditions (implantation energies and temperatures, tungsten material) are given in the figures. The reemission coefficient is defined as the ratio of the incoming non-reflected ion flux to the released flux of deuterium. The experimental data curves are described reasonably well, with the exception of the first phase of the reemission curves during keV implantation after the onset of the ion beam in Fig. 1. However, this is a consequence of the assumption of a preimplanted sample in the model calculations.

The rate coefficients for diffusion and recombination are obtained by fitting the isothermal released flux after the termination of the ion beam as well as the shape of the TDS spectra after the implantation. The deviations in the rate coefficients for single crystal tungsten and wrought tungsten in Table 1 are small, but calculating the released fluxes for the single crystal tungsten cases with the wrought tungsten parameter lead to completely disagreement with the experimental data and vice versa. The fitted rate coefficients for diffusion and recombination differ from the respective values in the literature [9,10,14], probably due the different experimental conditions, where thermal molecular and/or atomic hydrogen was offered to hot tungsten surfaces (> 1100 K).

The trap energies are obtained by fitting the temperature position of the TDS maxima. In the case of the keV implantation, both trap types are present, and the trap concentrations are obtained by fitting the experimental inventories. In the case of 100 eV implantation, the second peak which may also indicate a small amount of ion induced traps is not considered for the parameter fitting

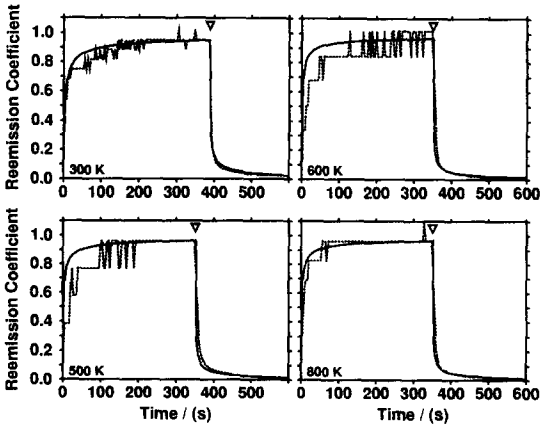

Fig. 2. Modeling of reemission data [6,13] for 100 eV D^+ implantation of wrought tungsten at 300 K, 500 K, 600 K, and 800 K, respectively, with a flux of 2×10^{19} D/(cm^2 s). Dotted lines denote experimental data, solid lines the computational results. The triangle denotes the ion beam termination time.

Table 1
Parameters used for the model calculations

Parameter	Tungsten material		Unit
	single crystal	wrought	
Surface recombination			
Preexp. factor	3.8×10^{3}	3×10^{1}	m $\sqrt{K}$ /s
Activation energy	0.35	0.31	eV
Diffusion			
Preexp. factor	3×10^{-10}	1.5×10^{-10}	m^2/s
Activation energy	0.25	0.25	eV
Natural traps			
Trap energy	0.5	0.5	eV
Concentration	6×10^{-3}	1×10^{-2}	traps/W
Ion induced traps	1.5, 8 keV D^+	100 eV D^+	
Trap energy	1.25	—	eV
Concentration	0.16	—	traps/W

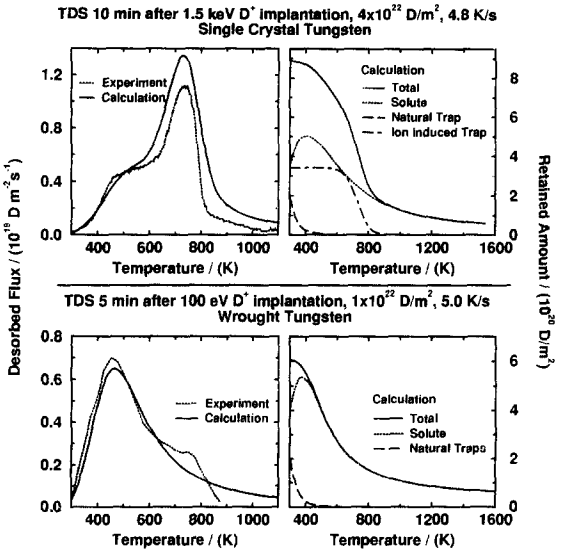

Fig. 3. Modeling of TDS spectra after implantation at 300 K and calculated deuterium inventories during TDS for (top) 1.5 keV D^+ with a fluence of 4×10^{22} D/m^2 [3], and (bottom) 100 eV D^+ with a fluence of 1×10^{22} D/m^2 [6].

due to the background problems mentioned in [6]. (The differences in the TDS spectra of Fig. 3 and the respective figure in [6] are caused by a different background subtracting of the original data.)

The first peak in the TDS spectra is associated with desorption of solute deuterium and deuterium bounded to the low energy natural traps, whereas the second peak is dominated by desorption of deuterium bounded to the high energy ion induced traps. From the fitting, we obtained a slightly increased natural trap concentration for wrought tungsten which may reflect the structural difference. The inventory measured by TDS depends very critically on the time between the ion beam termination and the onset of TDS due to the decrease of the solute inventory after the termination of the ion beam. This uncertainty may also cause the differences in the calculated and experimental TDS spectra in Fig. 3 for the 1.5 keV implantation case.

The parameter of Table 1 differs drastically from the model parameter in [6]. But this is a consequence of the large number of experimental data available now for this work — in contrast to reemission and TDS data of deuterium implanted with only a single energy and at a single temperature in [6] — and reflects the uncertainty of deriving model parameters from a limited experimental data base.

As a result of the calculations, recombination limits the hydrogen release through the front surface. The hydrogen flux decay rate after the termination of the ion beam is determined by the ratio of the recombination and diffusion coefficients. The decay rates are of the same order of magnitude (i.e. seconds) for all temperatures due to the small difference in the activation energies of diffusion and recombination coefficient. The solute concentration profile is constant up to a certain depth, defining the 'diffusion' zone, and decreasing to zero towards the back surface (for semi-infinite samples). As can be seen from Table 2, the

Table 2
Deuterium inventories, solute concentrations and depths in tungsten at the end of implantation at 300 K, obtained from model and TRIM calculations

	Tungsten material			
	single crystal		wrought	
Ion energy	1.5 keV	8 keV		100 eV
Implanted fluence ($D\ m^{-2}$)	4×10^{22}	2×10^{23}	1×10^{22}	1×10^{25}
Inventory ($D\ m^{-2}$)	1×10^{21}	5.2×10^{21}	9.8×10^{20}	4.4×10^{22}
Solute concentration	0.006 D/W	0.03 D/W	0.06 D/W	0.15 D/W
Constant down to	5.0 μm	5.0 μm	0.2 μm	2.5 μm
Mean ion range	16 nm	60 nm		4.3 nm
Depth of damage zone	35 nm	180 nm		—

depth of this diffusion zone exceeds the implantation zone by more than two orders of magnitude.

Fig. 3 also shows the calculated deuterium inventory during the thermal desorption runs. The solute fraction is of the same order of magnitude as the trapped one at room temperature and dominates the deuterium inventory. At 1600 K, about 10% of the initial deuterium content at 300 K — a few percent of the implanted fluence — is still solved in tungsten. The natural traps depopulate rather quickly with increasing temperature — they are filled to about 20% at room temperature — whereas deuterium bounded to the ion induced traps is (thermally) detrapped above about 600 K.

The experimental measured deuterium inventories of different tungsten modifications [3] depend on the material and on the time difference between the end of implantation and the analysis. The inventories determined by integrating the reemission curves and the TDS spectra show large differences. On the other hand, all analyzed tungsten materials have the same inventory of about 3×10^{20} D/m^2 days after the implantation with 1.5 keV D^+ [3]. At this time one can expect that most of the solute deuterium was already released and the inventory consists mainly of deuterium bounded to ion induced trapping sites. Hence, the measured material dependence of the deuterium inventory is due to changes in the solute deuterium inventory and with that in the rate coefficients. The results of Wang et al. [15] from reemission and TDS experiments during and after keV D^+ implantation of tungsten indicate that these changes can be attributed to the carbon impurity content of the tungsten material. The hydrogen inventory of carbon containing tungsten samples is enhanced by a factor of about 2. The same effect may cause the differences of the rate coefficients between single crystal and wrought tungsten: whereas single crystal tungsten has no impurities, wrought tungsten contains about 3% carbon [3]. As can be seen in Table 1, carbon seems to retard both diffusion and recombination, leading to an increasing solute, and hence, total deuterium inventory.

4. Consequences for the onset of tungsten as fusion reactor material

Fig. 4 shows calculated deuterium inventories during and after implantation of wrought tungsten with 100 eV D^+ for 1000 s and with a flux of 1×10^{22} D/(m^2 s), simulating the conditions in the ITER divertor [16]. The deuterium inventory is mainly dominated by the solute deuterium.

The high solute concentration of hydrogen is the main difference of tungsten compared to graphite, caused by the different recombination processes: For metals, recombination takes place at the geometrical surface. Hence, hydrogen has to diffuse to the surface to be released establishing the high solute concentration. In graphite, hydrogen atoms

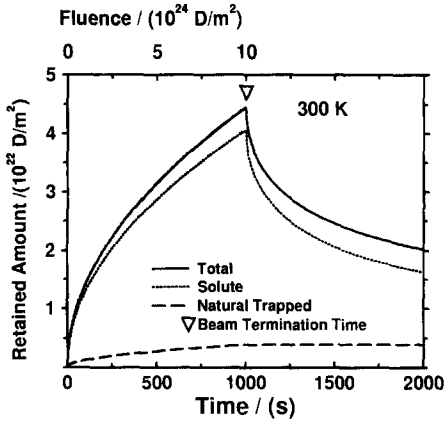

Fig. 4. Calculated deuterium inventories during and after 100 eV implantation of wrought tungsten with 1×10^{22} D/(m^2 s) at 300 K. The beam was switched on at zero and terminated at 1000 s.

recombine at inner surfaces, with a subsequent fast diffusion of the hydrogen molecules to the geometrical surface where they are immediately released. (For a discussion of hydrogen behavior in graphite see [17] and the references therein.) Hence, the solute inventory can be neglected in graphite, the hydrogen inventory at 1600 K being orders of magnitudes lower than at 300 K.

Due to the high solute concentration, hydrogen can accumulate in tungsten to very high inventories with increasing bombarding fluence without saturation fluence (as also seen in experiments [6–8]). For recombination limited release of hydrogen from tungsten, as it is the case for ion implantation, the solute inventory during implantation scales with the square root of the implantation fluence [6,7,18], but depends only slightly on the implantation energy (see Fig. 3). As mentioned above, carbon impurities in tungsten, introduced from the main plasma, may further increase the solute hydrogen inventory. In contrast, the hydrogen inventory in graphite increases above a certain saturation fluence only marginally with increasing implantation fluence by accessing natural traps beyond the implantation zone due to diffusion. An increase of the implantation fluence by three orders of magnitudes will change the hydrogen inventory in graphite only by 50% [19], but in tungsten by a factor of 30 (see also Table 2). Hydrogen will also accumulate in tungsten if the delay time between two plasma discharges is shorter than the time needed for the release of the solute hydrogen. The high amounts of solute hydrogen in tungsten may also change the thermal and mechanical properties of tungsten by phase changes and cause damage due to build-up of blisters and gas filled voids.

The high solute hydrogen concentration in tungsten has not only consequences for the controlling of the plasma particle balance, but also for the build up and the recycling of tritium in the vessel walls. Even a moderate sudden temperature increase of a tungsten target tile will release

large amounts of hydrogen into the plasma whereas the (trapped) hydrogen inventory in graphite will remain unchanged up to temperatures of 700 K. Tritium will accumulate in tungsten in much deeper regions than in graphite, and will also reach the back tungsten surface contaminating other structural materials. Accumulated tritium should be more easily expelled from graphite than from tungsten: temperatures of 1500 K are sufficient for the total release of hydrogen from graphite, whereas even at 1600 K tungsten retains large solute hydrogen inventories (Fig. 3).

5. Conclusion

The trapping and release of hydrogen implanted in tungsten can be summarized as follows:

– Hydrogen can be dissolved in large amounts in tungsten, the amount of solute hydrogen dominating the hydrogen inventory. The solute hydrogen inventory decreases only slightly with increasing temperature during thermal desorption: at 1600 K, about 10% of the initial hydrogen content retained at 300 K is still solved in tungsten.

– For the experimental conditions used in the calculations (energies up to 8 keV and fluxes of the order of 10^{19} D/(m^2 s), the hydrogen behavior is governed by recombination. This leads to a hydrogen 'diffusion' zone with constant solute concentrations more than two orders of magnitude larger than the implantation zone. Therefore, the solute hydrogen inventory depends only slightly on the ion incident energy but scales with the square root of the incident fluence.

– From TDS experiments, two trapping sites in tungsten can be derived: natural traps with energies of about 0.5 eV and concentrations of the order of 10^{-2} traps/W, and ion induced traps with energies of about 1.2 eV and concentrations of 0.16 traps/W, restricted to the implantation zone.

The high solute concentration of hydrogen is the main difference of tungsten compared to graphite. The resulting apparently unlimited accumulation of tritium deep in the bulk of tungsten down to the backward surface with increasing implantation fluence and number of plasma discharges, the possible release of tritium through the back surface, high tritium inventories even above 1500 K and a release of large amounts of hydrogen into the plasma due to small temperature changes disadvantage tungsten for the onset of tungsten as fusion reactor material with regard to hydrogen recycling properties.

Acknowledgements

We would like to thank Dr. M. Mayer and Dr. W. Eckstein for performing calculations on the implantation range of deuterium in tungsten with the TRIM program and Dr. J. Roth for valuable discussions.

References

[1] G. Janeschitz, J. Nucl. Mater. 220–222 (1995) 73.
[2] R. Neu, K. Asmussen, M. Bessenrodt-Weberpals, S. Deschka, R. Dux, W. Engelhardt, J.C. Fuchs, C. García-Rosales, A. Herrmann, S. Hirsch, F. Mast, K. Krieger, J. Roth, A. Thoma, U. Wenzel, the ASDEX Upgrade Team, the NI Team, the ICRH Team, and the ECRH Team, these Proceedings, p. 678.
[3] V.Kh. Alimov and B.M.U. Scherzer (1995), to be published.
[4] V.Kh. Alimov and B.N.U. Scherzer (1995), to be published.
[5] J.W. Davis and A.A. Haasz, J. Nucl. Mater. 223 (1995) 312.
[6] C. García-Rosales, P. Franzen, H. Plank, J. Roth and E. Gauthier, presented at 7th Int. Conf. on Fusion Reactor Materials, Obninsk, Russia, Sept. 1995.
[7] A.A. Pisarev, A.V. Varava and S.K. Zhdanov. J. Nucl. Mater. 220–222 (1995) 926.
[8] A.A. Haasz and J.W. Davis (1996), these Proceedings, p. 1076.
[9] K.L. Wilson, in: Data Compendium for Plasma–Surface Interactions (IAEA, Vienna, 1984).
[10] K. Kizu, T. Tanabe and K. Miyazaki, 7th Int. Conf. on Fusion Reactor Materials, Obninsk, Russia, September 1995, J. Nucl. Mater. (1996).
[11] W. Möller and J. Roth, in: Physics of Plasma–Wall Interactions in Controlled Fusion, D. Post and R. Behrisch, eds., Vol. 131, NATO ASI Series B (Plenum Press, New York, London, 1986).
[12] P. Franzen, to be published.
[13] H. Plank, Max-Planck-Institut für Plasmaphysik, Garching (1996), unpublished results.
[14] R. Frauenfelder, J. Vac. Sci. Technol. 6 (1969) 388.
[15] W. Wang, V.Kh. Alimov, B.M.U. Scherzer and J. Roth (1996), these Proceedings, p. 1087.
[16] A.F. Rowcliffe, A. Hishinuma, M.L. Grossbeck and S. Jitsukawa, J. Nucl. Mater. 179–181 (1991) 125.
[17] A.A. Haasz, P. Franzen, J.W. Davis, S. Chiu and C.S. Pitcher, J. Appl. Phys. 77 (1995) 66–86.
[18] B.L. Doyle, J. Nucl. Mater. 111–112 (1982) 628.
[19] A.A. Haasz and J.W. Davis, J. Nucl. Mater. 209 (1994) 155.